



Synthesis and Application of Reusable and Magnetic RGO/Fe₃O₄ Nanocomposites in BR46 Removal from an Aqueous Solution; Future Prospects of an Efficient Adsorption Platform

Fatemeh Habibi^{1,2}, Mirmehdi Seyyedi³, Bita Ayati^{2*}

¹Civil and Environmental Engineering Faculty, University of Texas at Arlington, USA

²Civil and Environmental Engineering Faculty, Tarbiat Modares University, Iran

³Department of Civil and Architectural Engineering, University of Wyoming, USA

*Corresponding author, Email address: Ayati_bi@modares.ac.ir

Received 28 June 2022,
Revised 11 Aug 2022,
Accepted 12 Aug 2022

Keywords

- ✓ BR46 adsorption
- ✓ RGO/Fe₃O₄ nanocomposites
- ✓ adsorbent regeneration
- ✓ adsorption isotherm

Ayati_bi@modares.ac.ir
Phone: +98; (21)82883328

Abstract

Application of adsorbents in removing dye contaminants from aqueous solutions have been of huge interest in recently. Despite having a descent adsorption potential, some limitations including the ones associated with their separation after the process and regeneration necessitate modifications through which these constraints are alleviated. Hereof, synthesis and application of an innovative and magnetic nanocomposite, namely reduced graphene oxide (RGO) coated with iron oxide (Fe₃O₄) was suggested for removal of BR46 dye from an aqueous solution. The nanocomposites were synthesized by a thoroughly-explained novel one-pot simplified co-precipitation method and their properties were characterized by X-ray diffraction (XRD) analysis, field emission scanning electron microscopy (Fe-SEM) images, and Fourier transform infrared spectroscopy (FT-IR) spectra. Process optimization for different factors was carried out using the central composite design (CCD). At its optimum condition ([RGO/Fe₃O₄]_{optimum}=0.46 g/L, [BR46]_{optimum}=33 mg/L, pH_{optimum}=7.7), 90.50% of BR46 removal was experimentally obtained after 120 minutes by the suggested system. the adsorption process was best described by the pseudo second-order model and the equilibrium data were best fitted into the Langmuir adsorption isotherm.

1. Introduction

Galloping rate of industrialization in recent decades has introduced a remarkable volume of wastewater to water bodies. Among different wastewater types, those consisting dyes have been considered serious threats to the environment for their irreparable effects. Dyes are organic compounds that are widely used in various industries as textile, paper, plastics, food, and tannery to name a few [1, 2, 3]. In this regard, more than 40,000 types of dyes and pigments are used in different industrial units, and about 450,000 of their species are generated annually. The application and production of these synthetic materials cause enormous amount of water loss [4]. Even a low concentration of dyes in water bodies (less than 1 ppm) can decrease their quality through changing their color, blocking sunlight radiation, and decreasing gas solubility [5, 6]. High level of dye consumption causes the discharge of large volumes of dyeing wastewater into the water resources, and also gives rise to serious problems for human health such as high heart beat rate, vomiting, and skin diseases [7, 8, 9, 10]. Therefore, the removal of these hazardous and toxic compounds prior to their discharge into the environment seems vital as it has been considered one of the top priorities in recent years. Since conventional wastewater treatment technologies are proven to be nearly ineffective for dye removal, novel treatment methods

in general and modern adsorption technologies as application of graphene-based adsorbents in particular have drawn great attention recently. Further development of such approaches is commonly encouraged for their higher removal efficiency, lower cost, and insensitivity to toxic substances [11].

Graphene is basically a two-dimensional layer of hexagonally (honeycomb) arranged carbon atoms which has been of great interest recently in both experimental and theoretical research thanks to its remarkable electrical-mechanical properties like high specific surface area [12, 13, 14]. As for its application in environmental engineering, the large delocalized π -electron system of graphene can allow having strong π - π interactions with the aromatic rings in most dyes. Thus, the advent of this one-atom-thick compound has suggested exciting opportunities for developing the next generation of adsorbents, since its discovery in 2004 [15, 16]. Despite their significant adsorption capacity, graphene-based adsorbents still have their drawbacks; the most important of which is the constraint associated with their separation from the solution after the process. This implies the necessity for certain modifications through which such constraints are at least partly alleviated.

In the past few years, application of nanotechnology in general and magnetic nanocomposites in particular for separation purposes has been of huge interest for their unusual structure, rapid separation, low cost, non-toxicity, and environmental benignity, among other specifications [17, 18, 19, 20, 21]. Nanocomposites are mostly composed of magnetic particles like iron, nickel, and cobalt along with their oxides [22]. Since introduction of magnetic properties into a graphene-based adsorbent like reduced graphene oxide (RGO) can offer a practical approach to overcome its separation difficulties from aqueous solutions, coating it with a magnetic composite was suggested as an innovative modification in this work.

Basic red 46 (BR46), a synthetic dye, is mainly used for dyeing polyacrylonitrile fiber and modified polyester in the industry. Its wide industrial application, mutagenicity, and carcinogenicity in human being motivated its usage in this study [5].

Taking all the aforementioned aspects into account, prospects of RGO/Fe₃O₄ nanocomposites for removal of BR46 from an aqueous solution was investigated in this research work. The nanocomposites were synthesized through a facile one-pot simplified precipitation method as described in the following sections.

Different statistical approaches could be followed in order to acquire the optimum operational conditions. The conventional optimization method, which is based on changing one factor while keeping the other factors constant (OFAT), is a time-consuming approach. Moreover, this method does not take the interactions between factors into account. Thus, it is necessary to choose a more efficient approach. The response surface methodology (RSM) is considered as one of the most accurate statistical techniques which could be used to optimize the performance of adsorption processes with minimal experimental effort [23, 24, 25, 26]. That said, the effect of different parameters was investigated by the RSM in this research.

2. Methodology

2.1 Chemicals and instruments

Graphene oxide was purchased from Nanosany Corporation (Mashhad, Iran). Chemicals including FeCl₂.4H₂O, FeCl₃.6H₂O, NaOH, NaBH₄, H₂SO₄, and ethanol were purchased from Merck (Germany). The stock solution (100 mg/L) of BR46 was prepared by dissolving 100 mg of BR46 in 1000 mL of distilled water. All the solutions were prepared by diluting the stock solution with distilled water, and fresh dilutions were used for all experiments. The pH of the working solutions was adjusted by adding appropriate volumes of dilute H₂SO₄ or NaOH solutions.

The concentration of dye solutions was measured using a UV-visible spectrophotometer (DR4000, Hach, Germany). The X-ray diffraction (XRD) pattern of the prepared nanocomposite samples was collected on a X'pert MPD X-ray diffractometer (Philips, Netherlands) setup once $\text{CuK}\alpha$ ($\lambda=1.54056 \text{ \AA}$) radiation was scanned with 0.02 % of speed, 40 kV of voltage, and 30 mA of current. The field emission scanning electron microscopy (Fe-SEM) images were taken on a Mira 3-XMU (Tescan, Czech Republic) setup, and the Fourier transform infrared spectroscopy (FT-IR) spectra were recorded on a Frontier FT-NIR/MIR (PerkinElmer, USA) Spectrometer. Moreover, the magnetic properties of the synthesized nanoparticles were analyzed using a vibrating sample magnetometer (DXV-100, Dexin, China) at the room temperature ($T=25\pm 1^\circ\text{C}$).

2.2 Synthesis of RGO/Fe₃O₄ magnetic nanocomposite

RGO/Fe₃O₄ magnetic nanocomposites were synthesized by a one-pot simplified co-precipitation method wherein the formation of superparamagnetic Fe₃O₄ nanoparticles and reduction of GO were carried out simultaneously. First, 50 mg of GO was added to 150 mL of deionized water and subjected to an ultrasonic dispersion (Q700 Sonicator, Qsonica, USA) for two hours. Secondly, 176 mg of FeCl₃.6H₂O and 130 mg of FeCl₂.4H₂O ($[\text{Fe}^{3+}]/[\text{Fe}^{2+}]=1$) were dissolved in 50 mL of deionized water and then added to the GO solution. The NaOH solution was gradually added dropwise to the solution until the pH was equal to 10. The solution was then heated to 80°C and stirred for two hours. Once the mixture was well-dispersed, the solution consisting 300 mg of NaBH₄ in 50 mL of distilled water was added slowly as the solution was stirred. Eventually, this process was continued for one hour at 80°C. The final product (RGO/Fe₃O₄ magnetic nanocomposite) was separated by magnet, washed with distilled water and ethanol for several times, and then dried at 60°C.

2.3 Adsorption experiments

Experiments were conducted in a custom-built plexiglass batch reactor capable of holding 25 mL of dye solution at the room temperature ($T=25\pm 1^\circ\text{C}$), which was placed on a platform shaker (New Brunswick Innova 40 series, Eppendorf, Germany) working at 200 rpm of mixing rate. The concentration of dye was determined by the spectrophotometer at 531 nm (λ_{max}) of wavelength. The dye removal percentage and the amount of dye removal per adsorbent weight were respectively calculated by [Eqn. 1-2](#).

$$R = (C_0 - C_e)/C_0 \times 100 \quad \text{Eqn. 1}$$

$$q_e = (C_0 - C_e)V/W \quad \text{Eqn. 2}$$

where C_0 (mg/L) represents the initial dye concentration, C_e (mg/L) is the dye equilibrium concentration, V (L) is the volume of the solution, and W (g) is the weight of the adsorbent (RGO/Fe₃O₄ magnetic nanocomposite). The adsorbent was removed from the solution by an external magnet after each experiment as shown in [Figure 1](#).



Figure 1. Illustration of BR46 removal by synthesized RGO/Fe₃O₄ nanocomposites and their separation from the solution by magnet.

2.4 Central Composite Design optimization

Response surface methodology in general and central composite design experimental design in particular were followed to acquire an optimal operational condition and determine the relationships between different input variables including adsorbent dosage, dye concentration, and solution pH. The Design Expert (Version: 7.0.0) statistical software was used in this study and the ranges and levels of input variables were as shown in **Table 1**. Also, **Table 2** provides a central composite design matrix with dye removal percentage as the response value once having 2n factorial points (n is the number of variables), 2n axial points, and 6 central points.

Table 1. Real values and coded levels of independent variables.

Factors	Coded levels				
	-2	-1	0	1	2
RGO/ Fe ₃ O ₄ dose (mg/L)	0.32	0.4	0.48	0.56	0.64
BR46 conc. (ppm)	10	20	30	40	50
pH	6	7	8	9	10

Table 2. Suggested CCD matrix and acquired values for BR46 removal (%).

Trial no	Variables in real values			BR46 removal (%)
	X ₁ (adsorbent dose) (mg/25 mL)	X ₂ (Initial BR46 Conc.) (ppb)	X ₃ (pH)	
1	10	40	9	78.49
2	12	30	8	97.69
3	12	30	6	97.78
4	8	30	8	78.11
5	12	10	8	100
6	12	30	8	97.09
7	14	20	9	100
8	12	30	8	97.66
9	12	50	8	72.30
10	16	30	8	98.36
11	12	30	8	98.14
12	12	30	8	93.59
13	10	20	7	98.40
14	14	20	7	100
15	10	40	7	77.79
16	10	20	9	98.95
17	14	40	7	92.49
18	12	30	10	95.69
19	12	30	8	94.36
20	14	40	9	84.32

In this regard and considering the defined number of variables and ranges, 20 experiments with different conditions were suggested by the software. Also, based on the analysis of variance (ANOVA), a second-order quadratic polynomial model (Eqn. 3) was proposed to predict the BR46 removal% and estimate the coefficients by correlating the interactions between the process variables and responses.

$$Y(\%) = \beta_0 + \sum_{i=1}^3 \beta_i X_i + \sum_{i=1}^3 \sum_{j=1}^3 \beta_{ij} X_i X_j + \sum_{i=1}^3 \beta_{ii} X_i^2 \quad \text{Eqn. 3}$$

where Y is the predicted response (removal percentage), X_i is the value for independent variables, and β_0 is the constant. Moreover, β_i , β_{ii} , and β_{ij} respectively stand for the linear, quadratic, and interaction coefficients.

3. Results and Discussion

3.1 Characterization of RGO/Fe₃O₄ nanocomposites

The Fe-SEM image of synthesized nanocomposites was as illustrated in Figure 2. As seen in, the Fe₃O₄ nanoparticles with an approximate size of 20 nm were well-distributed on the surface of RGO layers.

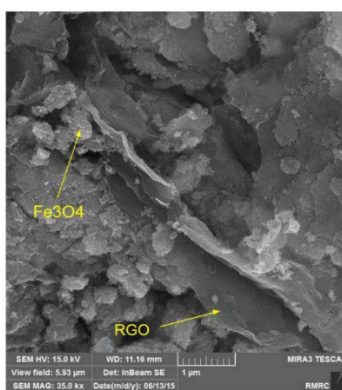


Figure 2. Fe-SEM image of synthesized RGO/Fe₃O₄ nanocomposites.

The XRD analysis was also exploited to investigate the phase and structure of RGO/Fe₃O₄ nanocomposites. As seen in Figure 3, the XRD pattern of synthesized nanocomposites showed six diffraction lines at $2\theta=35.2^\circ$, $2\theta=41.53^\circ$, $2\theta=50.7^\circ$, $2\theta=63.28^\circ$, $2\theta=67.75^\circ$, and $2\theta=74.52^\circ$ which were very similar to those of Fe₃O₄ nanoparticles. The absence of diffraction lines representative of GO and broad peaks, respectively located at $2\theta=11.94^\circ$ and $2\theta=21^\circ$, confirmed the formation of reduced graphene and prevention of reduced graphene oxide sheets from sticking together.

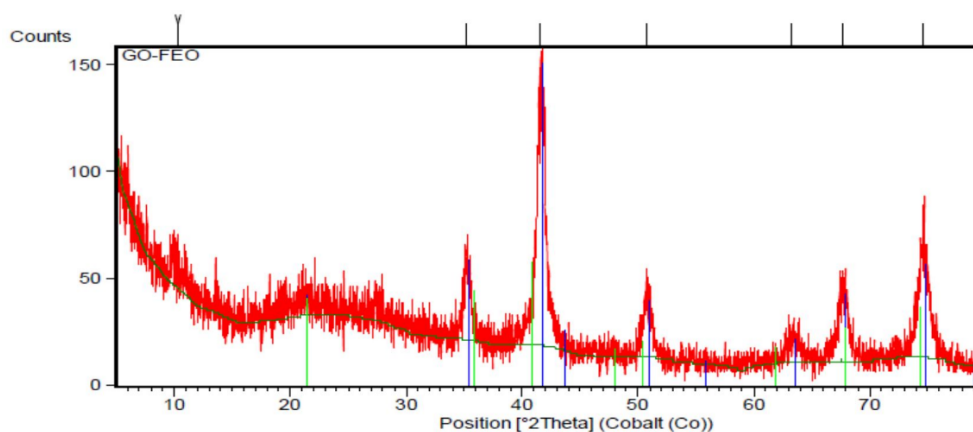


Figure 3. XRD pattern of synthesized RGO/Fe₃O₄ nanocomposites.

The FT-IR spectra was used to characterize the formation of both graphene oxide and RGO/Fe₃O₄ powders and the results were as shown in **Figure 4**. As for the GO, the spectrum showed the characteristic peaks of O–H ($\nu_{\text{O-H}}$ at 3177), C=C ($\nu_{\text{C=C}}$ at 1621), C–O ($\nu_{\text{C-O}}$ at 1049), and C=O ($\nu_{\text{C=O}}$ at 1733.51). With regards to the FT-IR spectrum for RGO/Fe₃O₄ powder, there was a significant reduction in the characteristic absorption band intensities of $\nu_{\text{O-H}}$, $\nu_{\text{C-O}}$, and $\nu_{\text{C=O}}$ (oxygen functionalities bands). Furthermore, the formation of a characteristic peak at 568 cm⁻¹ (C–Fe) was demonstrated.

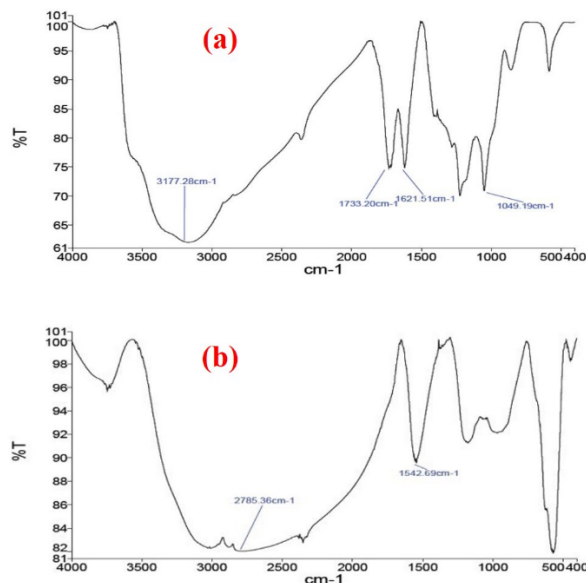


Figure 4. FT-IR spectra of; (a) GO and (b) synthesized RGO/Fe₃O₄ nanocomposites.

Considering the importance of magnetic properties in nanocomposites for their easy separation under the influence of magnetic field, the magnetic intensity of synthesized RGO/Fe₃O₄ nanocomposites was analyzed by the VSM at the room temperature ($T=25\text{ }^{\circ}\text{C}$). **Figure 5** shows the magnetization of synthesized nanocomposites as a function of applied magnetic field. As seen, a saturation magnetization intensity of 22.6 emu.g⁻¹ was acquired, which is sufficient for magnetic separation using an external magnet field.

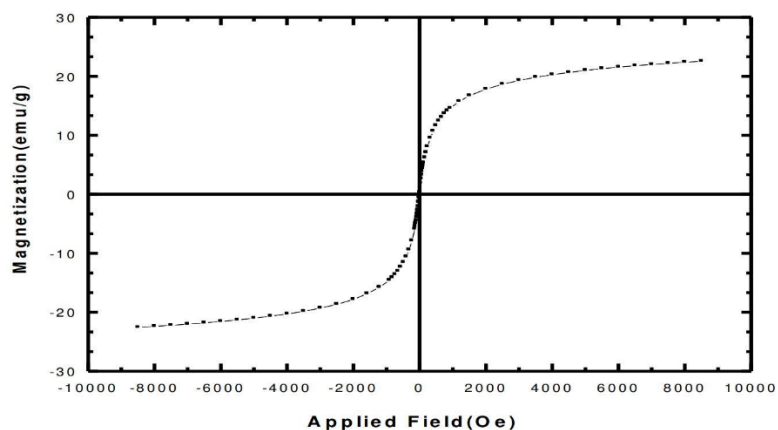


Figure 5. Magnetization curve of synthesized RGO/Fe₃O₄ nanocomposites.

3.2 Central Composite Design results

Eqn. 4 shows a second-order polynomial expression attained from the analysis of variance at 95% of confidence level ($p<0.05$):

$$\begin{aligned}
 Y(\%) = & 96.32 + 3.98X_1 - 7.48X_2 - 0.69X_3 \\
 & - 2.1X_1^2 - 2.62X_2^2 + 0.25X_3^2 \\
 & + 2.23X_1X_2 - 1.18X_1X_3 - 1X_2X_3
 \end{aligned}
 \tag{Eqn. 4}$$

where Y, X₁, X₂, and X₃ respectively represent dye removal (%), RGO/Fe₃O₄ nanocomposite dose (mg/25 mL), initial dye concentration (mg/L), and pH value.

The ANOVA was also used to evaluate the model's significance and adequacy respectively through the F-value and p-value which were obtained by analyzing the experimental data listed in [Table 3](#) [27]. A very high F-value ($F_{\text{model}}=30.78$) and a very low probability value ($P_{\text{model}}=<0.0001$) indicated that the acquired model was highly significant and adequate. The accuracy of the polynomial model was also appraised by the coefficient of determination ($R^2=0.9652$) as a criterion of deviation around the mean. Moreover, the rather large value of the adjusted determination coefficient ($R^2=0.9338$) indicated a good agreement between the experimental and predicted data.

The corresponding p-value of each term could be considered as a criterion which reflects its significance. Specifically, the removal efficiencies of BR46 were significantly affected by the linear effects of nanocomposite dose (X₁), dye concentration (X₂), their interactive term (X₁X₂), and quadratic terms (X₁² and X₂²) with p-values of respectively equal to 0.0001, 0.0207, 0.001, and 0.0002. The linear term of pH (X₃), its quadratic term (X₃²), and the other interactive terms between the parameters were found to have insignificant effects on the response. The plot depicting the predicted versus observed responses ([Figure 6](#)) indicated a good agreement between the acquired and anticipated values. This verified the reliability of the employed model.

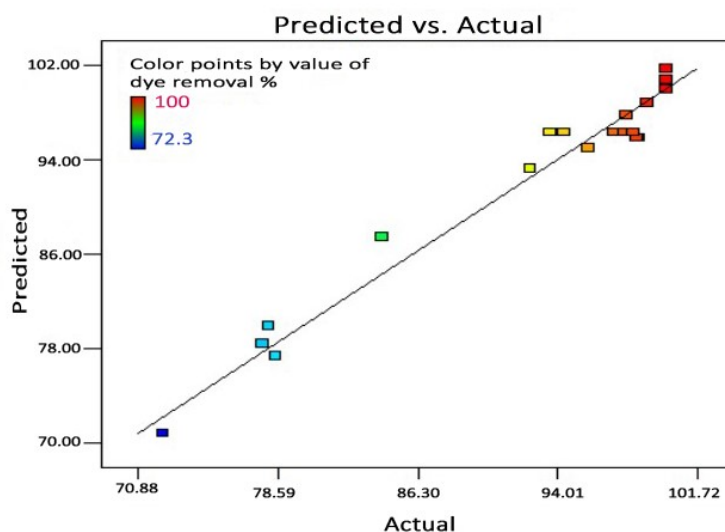


Figure 6. Experimentally acquired versus predicted values of BR46 removal.

Moreover, the contour plots in [Figure 7](#) represented a more detailed illustration for the effects of parameters including adsorbent dose, initial dye concentration, pH, and their interactions on BR46 removal. Indeed, [Figures 7a-c](#) are the graphical representations of [Eqn. 4](#). As shown in [Figure 7a](#), BR46 removal was enhanced with an increase in nanocomposite and diminished with an increase in initial dye concentrations. This can be described by the limited adsorption capacity of synthesized nanoparticles and their likely saturation once having high adsorbate to adsorbent ratios. These observations were also in accordance with the results shown in [Figure 7b](#) and [Figure 7c](#). pH is one of the main factors that can affect the performance of most adsorbents. The reason for choosing the studied pH range of 6 to 10 is that this has been already observed by other authors and also in this work that adsorption efficiency is lower in acidic media [28, 29]. In fact, an increase in pH leads to a rise in the

number of negative charges on nanocomposites surface and, in turn, boosts the electrostatic forces between the adsorbent and the adsorbate. However, as seen in **Figure 7b** and **Figure 7c**, BR46 removal did not significantly change when pH was increased from 6 to 10. This can be explained by the partly neutralized positive charges of dye molecules which could be caused by the formation of some bonds between hydroxide ions and their nitrogen atoms [30].

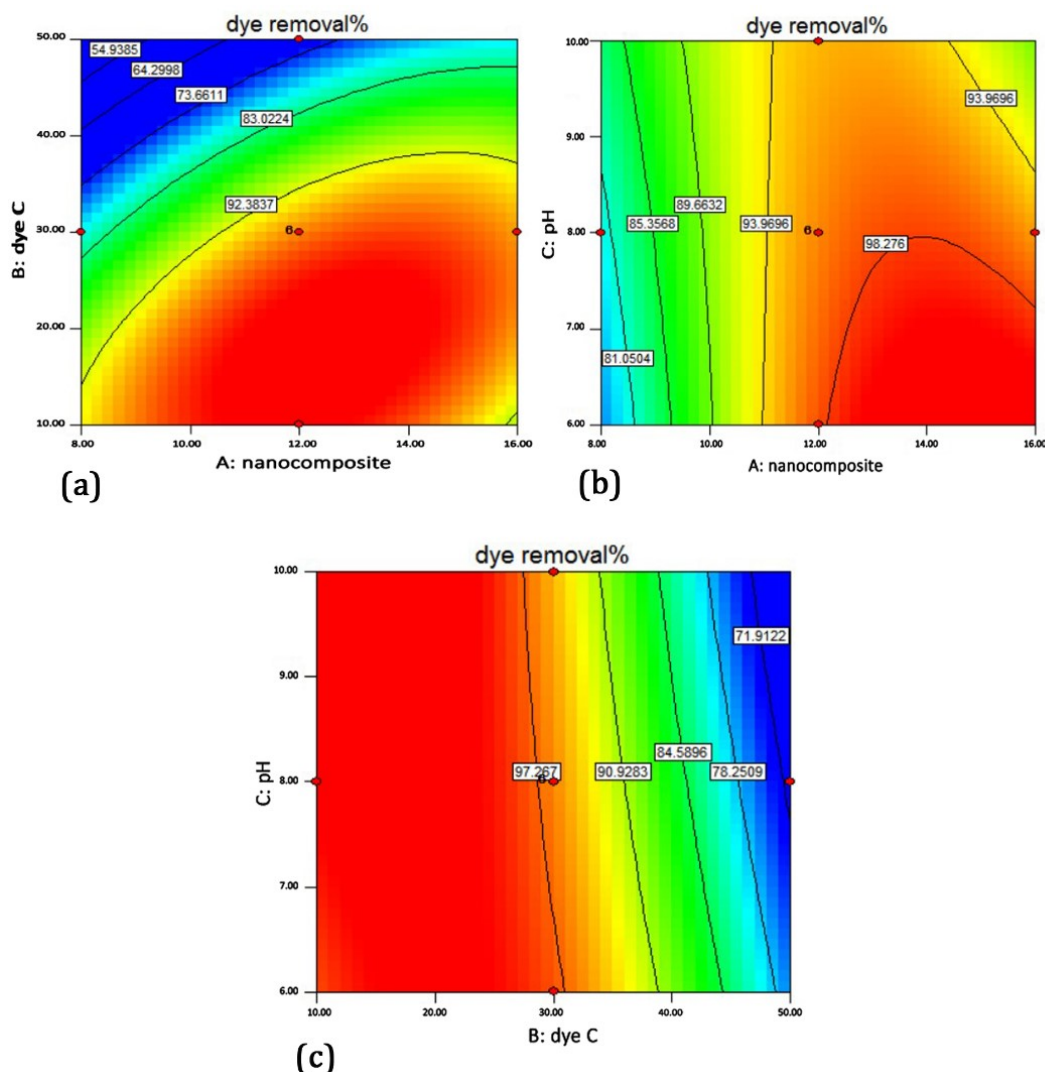


Figure 7. Contour plots for BR46 removal (%); (a) X_1 ([RGO/Fe₃O₄]) vs. X_2 ([BR46]) in fixed X_3 (pH), (b) X_1 ([RGO/Fe₃O₄]) vs. X_3 (pH) in fixed X_2 ([BR46]), and (c) X_2 ([BR46]) and X_3 (pH) in fixed X_1 ([RGO/Fe₃O₄]).

At its optimum condition ($[RGO/Fe_3O_4]_{\text{optimum}}=0.46$ g/L, $[BR46]_{\text{optimum}}=33$ mg/L, $pH_{\text{optimum}}=7.7$), 90.50% of BR46 removal was experimentally obtained after 120 minutes (adsorption equilibrium time) from the aqueous solution by the suggested system. The software also predicted 92.51% of BR46 removal at this very same condition and after similar time. As for the possible changes in solution pH during the process, not a significant shift was observed and a final pH value of 7.8 was acquired after 120 minutes.

3.3 Regeneration

The regeneration capability of any adsorbent plays an important role in expanding its industrial application. In other words, not only should an adsorbent have a high absorption capacity, but its total cost should also be low thanks to its desorption and regeneration potential. As already mentioned,

nanocomposites were separated by a magnetic field and then washed by ethanol to be regenerated and reused in this research. The adsorption capacity of synthesized nanocomposites for first five adsorption-desorption cycles were as shown in **Figure 8**. As seen, even after 4 cycles of regeneration, more than 80% percent of initial dye removal capacity at the optimum condition (90.50%) was achievable. Such observations highlight the regeneration capacity and industrial application prospects of synthesized adsorbents.

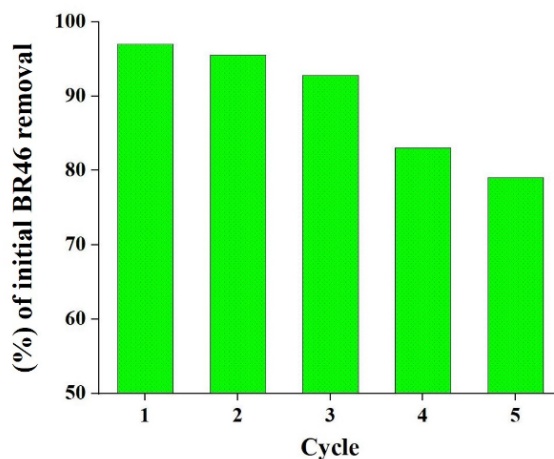


Figure 8. Ratio of BR46 removal (%) to initial efficiency in different cycle numbers.

3.4 Kinetic analysis

It is of great significance to study the adsorption mechanisms mainly by which the adsorption and desorption rates are controlled. That said, the rate of dye adsorption by synthesized RGO/Fe₃O₄ nanocomposites was studied as the kinetics were analyzed using the pseudo-first-order and pseudo-second-order kinetic models [31, 32]. The pseudo-first-order and pseudo-second-order kinetic equations were as respectively described in **Eqns. 5-6**:

$$\ln(q_e - q_t) = \ln q_e - k_1 t \quad \text{Eqn. 5}$$

$$t/q_t = 1/k_2 q_e^2 + 1/q_e \quad \text{Eqn. 6}$$

where k_1 (1/min) and k_2 (g/mg.min) respectively represent the equilibrium rate constants of pseudo-first-order and pseudo-second-order equations. Also, q_t and q_e represent the amounts of adsorbed dye respectively at the time t (min) and in the equilibrium state. **Table 4** represents the results for fitting the data to pseudo-first-order and pseudo-second-order kinetic models..

Table 4. Acquired values for decisive parameters of pseudo-first-order and pseudo-second-order models.

Models	Parameters	Values
Pseudo-first-order model	k_1 (1/min)	0.0503
	q_e (mg/g)	41.32
	R^2	0.9735
Pseudo-second-order model	k_2 (g/mgmin)	0.0020
	q_e (mg/g)	68.96
	R^2	0.9999

In this regard, and as for the pseudo second-order model, a meaningful linear relationship between t/q_t and t was obtained once having a correlation coefficient of 0.9999. This implies the appropriateness and applicability of the pseudo second-order model to describe the adsorption process. The values of q_e and k_2 were respectively equal to 68.96 and 0.002 in this model

3.5 Adsorption isotherms

In order to better understand the interactions between the adsorbent and adsorbate, different adsorption isotherms were studied. In this respect, equilibrium data were analyzed using a number of widely used isotherms including Langmuir, Freundlich, Temkin, and Dubinin-Radushkevich [33, 34, 35, 36]. The Langmuir isotherm suggests a quantitative description of a layer formation adsorbed on the outer surface of an adsorbent when further adsorption is not taking place. This isotherm is valid for a monolayer adsorption on a surface with certain number of identical positions. Mathematical description of this isotherm is as presented in Eqn. 7:

$$C_e/q_e = C_e/q_{max} + 1/q_{max}a_L \quad \text{Eqn. 7}$$

where C_e (mg/L) is the equilibrium concentration of the dye in the solution, q_e and q_{max} (mg/g) are the conventional and maximum adsorption capacities, and a_L is the Langmuir constant. The important feature of the Langmuir isotherm can be expressed by a dimensionless constant known as the separation factor which is defined as shown in Eqn. 8:

$$R_L = 1/(1 + a_L C_0) \quad \text{Eqn. 8}$$

where C_0 (mg/L) is the initial dye concentration. An R_L value within the range $0 < R_L < 1$ would indicate the favorability of adsorption in this work.

The Freundlich isotherm is applicable for heterogeneous energy levels and can be used for multilayer adsorption processes. This isotherm is mathematically defined as described in Eqn. 9:

$$\ln q_e = (1/n) \ln C_e + \ln K_F \quad \text{Eqn. 9}$$

where K_F and $1/n$ are respectively the Freundlich constant and heterogeneity factor. While an n value equal to 1 represents a linear adsorption, a value within the range $0 < n < 1$ implies a slow process. On the other hand, if $n > 1$, adsorption is favorable.

According to the Temkin isotherm, the adsorption energy is a linear function of the surface coverage. This isotherm is modeled as described in Eqn. 10:

$$q_e = B \ln K_T + B \ln C_e \quad \text{Eqn. 10}$$

$$B = (RT)/b$$

where K_T (L/mg) is the Temkin isotherm constant, R (8.314 J/mol.K) is the universal gas constant, T (K) is the absolute temperature, and b is the energy constant.

The values of all parameters in aforementioned equations for different isotherms were obtained from the slopes and intercepts of the linear plots including C_e/q_e versus C_e , $\ln q_e$ versus $\ln C_e$, and $\ln q_e$ versus $[RT \ln(1+1/C_e)]^2$. The results were as listed in Table 5. According to the drawn results, BR46 adsorption on synthesized RGO/Fe₃O₄ nanocomposites is best described by the Langmuir isotherm. In other words, formation of a dye monolayer on outer surface of nanocomposites is the most likely mechanism responsible for BR46 removal from the aqueous solution in this work.

Table 5. Acquired values for decisive parameters of different isotherms.

Models	Parameters	Values
Langmuir	a_L (L/mg)	2.053
	q_{\max} (mg/g)	63.93
	R^2	0.9987
Freundlich	K_F (L/mg)	40.73
	$1/n$	0.17
	R^2	0.9829
Temkin	K_T (L/mg)	1194
	B (kJ/mol)	6.3
	R^2	0.9558
Dubinin-Radushkevich	q_d (mg/g)	54.33
	B_D	9×10^{-9}
	R^2	0.8453

4 Conclusion

In this research, synthesis and application of an efficient and novel adsorbent, namely RGO/Fe₃O₄ nanocomposite, was evaluated in removal of BR46 dye contaminant from an aqueous solution. In fact, the combination of magnetic properties with those of graphene-based materials, provided an effective adsorption platform which was not only proven to have significant dye removal potential, but easily regeneratable through separation with a magnetic field and being washed by ethanol. The effects of various factors on adsorption process were optimized by the central composite design, and at their optimum values ($[RGO/Fe_3O_4]_{\text{optimum}}=0.46$ g/L, $[BR46]_{\text{optimum}}=33$ mg/L, $pH_{\text{optimum}}=7.7$), 90.50% of BR46 removal was experimentally acquired after 120 minutes from the aqueous solution. Interestingly, more than 80% of initial BR46 removal efficiency (90.50%) of synthesized nanocomposites was still obtainable even after 4 regeneration cycles thanks to their reusability advantages. The adsorption process was best described by the pseudo second-order model and the equilibrium data were best fitted into the Langmuir adsorption isotherm.

Aforementioned aspects of synthesized nanocomposites certainly highlight their future prospects for vast industrial applications, specially due to their regeneration capacity.

Disclosure statement *Conflict of Interest:* The authors declare that there are no conflicts of interest.

Compliance with Ethical Standards: This article does not contain any studies involving human or animal subjects.

References

1. R. Rahmati, B. Nayebi, and B. Ayati, Investigating the effect of hydrogen peroxide as an electron acceptor in increasing the capability of slurry photocatalytic process in dye removal. *Water Science and Technology*, 83(10) (2021) 2414-2423. <https://doi.org/10.2166/wst.2021.136>
2. S.C.M. Signorelli, J.M. Costa, and A.F.d.A. Neto, Electrocoagulation-flotation for orange II dye removal: Kinetics, costs, and process variable effects. *Journal of Environmental Chemical Engineering*, 9 (2021) 106157. <https://doi.org/10.1016/j.jece.2021.106157>

3. J. Fang, Y. Chen, C. Fang, and L. Zhu, Regenerable adsorptive membranes prepared by mussel-inspired co-deposition for aqueous dye removal. *Separation and Purification Technology*, 281 (2022) 119876. <https://doi.org/10.1016/j.seppur.2021.119876>
4. E. Routoula, and S.V. Patwardhan, Degradation of anthraquinone dyes from effluents: a review focusing on enzymatic dye degradation with industrial potential. *Environmental Science and Technology*, 54(2) (2022) 647-664. <https://doi.org/10.1021/acs.est.9b03737>
5. A. Malik, and E. Grohmann, Environmental protection strategies for sustainable development, Springer, ISBN : 978-94-007-1591-2 (2012).
6. A. Azari, R. Nabizadeh, S. Nasser, A.H. Mahvi, and A.R. Mesdaghinia, Comprehensive systematic review and meta-analysis of dyes adsorption by carbon-based adsorbent materials: Classification and analysis of last decade studies. *Chemosphere*, 250 (2020) 126238. <https://doi.org/10.1016/j.chemosphere.2020.126238>
7. G. Sharma, M. Naushad, A. Kumar, S. Rana, S. Sharma, A. Bhatnagar, F.J. Stadler, A.A. Ghfar, and M.R. Khan, Efficient removal of coomassie brilliant blue R-250 dye using starch/poly (alginic acid-cl-acrylamide) nanohydrogel. *Process Safety and Environmental Protection*, 109 (2017) 301-310. <https://doi.org/10.1016/j.psep.2017.04.011>
8. P.C. Nagajyothi, L.V. Reddy, K.C. Devarayapalli, S.P. Vattikuti, Y.J. Wee, and J. Shim, Environmentally friendly synthesis: photocatalytic dye degradation and bacteria inactivation using Ag/f-MWCNTs Composite. *Journal of cluster Science*, 32 (2020) 711-718. <https://doi.org/10.1007/s10876-020-01821-8>
9. E. Mourid, M. Lakraimi, E. El Khattabi, L. Benaziz, and M. Berraho, Removal of textile dye acid green from wastewater by activated carbon. *Journal of Materials and Environmental Science*, 8(9) 2017 3121-3130.
10. A.A. Zahrani, and B. Ayati, Improving Fe-based heterogeneous Electro-Fenton nano catalyst using transition metals in a novel orbiting electrodes reactor. *Chemosphere*, 256 (2020) 127049. <https://doi.org/10.1016/j.chemosphere.2020.127049>
11. V. Katheresan, J. Kansedo, and S.Y. Lau, Efficiency of various recent wastewater dye removal methods: a review. *Journal of Environmental Chemical Engineering*, 6(4) (2018) 4676-4697. <https://doi.org/10.1016/j.jece.2018.06.060>
12. J. Phiri, P. Gane, and T.C. Maloney, General overview of graphene: Production, properties and application in polymer composites. *Materials Science and Engineering B: Solid-State Materials for Advanced Technology*, 215 (2017) 9-28. <https://doi.org/10.1016/j.mseb.2016.10.004>
13. Y. Vasseghian, E. Dragoi, F. Almomani, V.T. Le, and M. Berkani, Graphene-based membrane techniques for heavy metal removal: A critical review. *Environmental Technology and Innovation*, 24 (2021) 101863. <https://doi.org/10.1016/j.eti.2021.101863>
14. S. Verma, and K. Kim, Graphene-based materials for the adsorptive removal of uranium in aqueous solutions. *Environment International*, 158 (2022) 106944. <https://doi.org/10.1016/j.envint.2021.106944>
15. K.P. Loh, Q. Bao, P.K. Ang, and J. Yang, The chemistry of graphene. *Journal of Materials Chemistry*, 20 (12) (2010) 2277-2289. <https://doi.org/10.1039/B920539J>
16. B. Mao, B. Sidhureddy, A.R. Thirupathi, P.C. Wood, and A. Chen, Efficient dye removal and separation based on graphene oxide nanomaterials. *New Journal of Chemistry*, 44 (11) (2020) 4519-4528. <https://doi.org/10.1039/C9NJ05895H>
17. J.L. Gong, B. Wang, G.M. Zeng, C.P. Yang, C.G. Niu, Q.Y. Niu, W.J. Zhou, and Y. Liang, Removal of cationic dyes from aqueous solution using magnetic multi-wall carbon nanotube

- nanocomposite as adsorbent. *Journal of Hazardous Materials*, 164 (2-3) (2009) 1517-1522. <https://doi.org/10.1016/j.jhazmat.2008.09.072>
18. L. Yu, H. Wu, B. Wu, Z. Wang, H. Cao, C. Fu, and N. Jia, Magnetic Fe₃O₄-reduced graphene oxide nanocomposites-based electrochemical biosensing. *Nano-Micro Letters*, 6(3) (2014) 258-267. <https://doi.org/10.5101/nml140028a>
 19. G. Simonsen, M. Strand, and G. Øye, Potential applications of magnetic nanoparticles within separation in the petroleum industry. *Journal of Petroleum Science and Technology*, 165 (2018) 488-495. <https://doi.org/10.1016/j.petrol.2018.02.048>
 20. E.F. Afshar, and M.A. Taher, New fabrication of CuFe₂O₄/PAMAM nanocomposites by an efficient removal performance for organic dyes: Kinetic study. *Environmental Research*, 204 (2022) 112048. <https://doi.org/10.1016/j.envres.2021.112048>
 21. M. Seyyedi, and B. Ayati, Treatment of petroleum wastewater using a sequential hybrid system of electro-Fenton and NZVI slurry reactors, future prospects for an emerging wastewater treatment technology. *International Journal of Environment and Waste Management*, 28(3) (2021) 328-348. <https://doi.org/10.1504/IJEW.2021.118369>
 22. H. Ravishankar, J. Wang, L. Shu, and V. Jegatheesan, Removal of Pb (II) ions using polymer based graphene oxide magnetic nano-sorbent. *Process Safety and Environmental Protection*, 104(B) (2016) 472-480. <https://doi.org/10.1016/j.psep.2016.04.002>
 23. X.J. Hu, Y.G. Liu, H. Wang, A.W. Chen, G.M. Zeng, S.M. Liu, Y.M. Guo, X. Hu, T.T. Li, Y.Q. Wang, and L. Zhou, Removal of Cu (II) ions from aqueous solution using sulfonated magnetic graphene oxide composite. *Separation and Purification Technology*, 108 (2013) 189-195. <https://doi.org/10.1016/j.seppur.2013.02.011>
 24. M. Zendehtdel, B. Shoshtari-Yeganeh, H. Khanmohamadi, and G. Cruciani, Removal of fluoride from aqueous solution by adsorption on NaP: HAp nanocomposite using response surface methodology. *Process Safety and Environmental Protection*, 109 (2017) 172-191. <https://doi.org/10.1016/j.psep.2017.03.028>
 25. T. Kumar, R. Mohsin, Z.A. Majid, M.F.A. Ghafir, and A.M. Wash, Experimental study of the anti-knock efficiency of high-octane fuels in spark ignited aircraft engine using response surface methodology. *Applied Energy*, 259 (2020) 114150. <https://doi.org/10.1016/j.apenergy.2019.114150>
 26. J.R. Hanumanthu, G. Ravindiran, R. Subramanian, and P. Saravanan, Optimization of process conditions using RSM and ANFIS for the removal of Remazol Brilliant Orange 3R in a packed bed column. *Journal of Indian Chemical Society*, 98 (2021) 100086. <https://doi.org/10.1016/j.jics.2021.100086>
 27. I.A. Appavoo, J. Hu, Y. Huang, S.F.Y. Li, and S.L. Ong, Response surface modeling of Carbamazepine (CBZ) removal by Graphene-P25 nanocomposites/UVA process using central composite design. *Water Research*, 57 (2014) 270-279. <https://doi.org/10.1016/j.watres.2014.03.007>
 28. M. Ghaedi, A.M. Ghaedi, M. Hossainpour, A. Ansari, M.H. Habibi, and A.R. Asghari, Least square-support vector (LS-SVM) method for modeling of methylene blue dye adsorption using copper oxide loaded on activated carbon: Kinetic and isotherm study. *Journal of Industrial and Engineering Chemistry*, 20(4) (2014) 1641-1649. <https://doi.org/10.1016/j.jiec.2013.08.011>
 29. V. Chandra, J. Park, Y. Chun, J.W. Lee, I.C. Hwang, and K.S. Kim, Water-dispersible magnetite-reduced graphene oxide composites for arsenic removal. *ACS Nano*, 4(7) (2010) 3979-3986. <https://doi.org/10.1021/nn1008897>

30. H. Sun, L. Cao, and L. Lu, Magnetite/reduced graphene oxide nanocomposites: One step solvothermal synthesis and use as a novel platform for removal of dye pollutants. *Nano Research*, 4(6) (2011) 550-562. <https://doi.org/10.1007/s12274-011-0111-3>
31. S.K. Lagergren, About the theory of so-called adsorption of soluble substances. *Kungliga Svenska Vetenskapsakademiens Handbook*, 24 (1898) 1-39.
32. Y.S. Ho, G. McKay, D.A.J. Wase, and C.F. Forster, Study of the sorption of divalent metal ions on to peat. *Adsorption Science and Technology*, 18(7) (2000) 639-650. <https://doi.org/10.1260/0263617001493693>
33. H. Freundlich, Adsorption in solutions. *Journal of Physical Chemistry*, 57(1) (1907) 385-470. <https://doi.org/10.1515/zpch-1907-5723>
34. I. Langmuir, The adsorption of gases on plane surfaces of glass, mica and platinum. *Journal of American Chemical Society*, 40(9) (1918) 1361-1403. <https://doi.org/10.1021/ja02242a004>
35. A. Damjanovic, and V. Brusic, V. Electrode kinetics of oxygen reduction on oxide-free platinum electrodes. *Electrochimica Acta*, 12(6) 1967 615-628. [https://doi.org/10.1016/0013-4686\(67\)85030-8](https://doi.org/10.1016/0013-4686(67)85030-8)
36. M.M. Dubinin, and H.F. Stoeckli, Homogeneous and heterogeneous micropore structures in carbonaceous adsorbents. *Journal of Colloid and Interface Science*, 75(1) (1980) 34-42. [https://doi.org/10.1016/0021-9797\(80\)90346-X](https://doi.org/10.1016/0021-9797(80)90346-X)

(2022) ; <http://www.jmaterenvironsci.com>